An empirical model of Saturn's bow shock: Cassini observations of shock location and shape

A. Masters,[1] N. Achilleos,[2] M. K. Dougherty,[1] J. A. Slavin,[3] G. B. Hospodarsky,[4] C. S. Arridge,[5,6] and A. J. Coates[5,6]

Received 7 April 2008; revised 9 June 2008; accepted 23 July 2008; published 17 October 2008.

[1] We present a new empirical model of Saturn's bow shock that utilizes observations from the Cassini spacecraft. Shock crossings are identified in magnetic field and plasma observations made by Cassini between June 2004 and August 2005. The Cassini crossings are then combined with the crossings made during the Saturn flybys of Pioneer 11, Voyager 1, and Voyager 2. Solar wind dynamic pressures for the Cassini crossings are estimated using upstream electron densities determined from Langmuir wave observations made by the Radio and Plasma Wave System. The crossing positions are rotated into aberrated coordinates to correct for the effect of the planet's orbital motion. In the case of Saturn this rotation is by $\sim 1°$. To correct for solar wind dynamic pressure variations, the crossing positions are normalized to the average pressure $\langle P_{SW} \rangle$ = 0.048 nPa. The model is then obtained by fitting a conic section to the crossings using a nonlinear least squares technique. To validate the assumptions made in constructing the model, we treat the parameters previously assumed to be constants as variables and fit their values using an optimization routine; this leads to a conic section that is within the positional uncertainty of the model. The spacecraft trajectories are considered, and we conclude that they do not significantly bias the model. The new model is compared to the existing models, and the similarities and differences are discussed. We suggest that the new model gives the most accurate empirical representation of the shape and location of Saturn's bow shock.

Citation: Masters, A., N. Achilleos, M. K. Dougherty, J. A. Slavin, G. B. Hospodarsky, C. S. Arridge, and A. J. Coates (2008), An empirical model of Saturn's bow shock: Cassini observations of shock location and shape, *J. Geophys. Res.*, *113*, A10210, doi:10.1029/2008JA013276.

1. Introduction

[2] The Cassini spacecraft's orbital tour at Saturn has allowed us to study the Kronian magnetosphere in more detail than ever before [*Matson et al.*, 2002]. Understanding of this complex system in the pre-Cassini era was based on data taken by the Pioneer and Voyager spacecraft as they flew by the planet [*Acuña and Ness*, 1980; *Smith et al.*, 1980; *Stone and Miner*, 1981, 1982; *Connerney et al.*, 1982]. Cassini has greatly increased the number of observations of the various plasma boundaries and has revealed a more complex picture of the configuration and dynamics of the magnetosphere. In situ measurements made by Cassini in the solar wind allow us to investigate the solar wind flow around the magnetospheric obstacle.

[3] The properties of the solar wind at Saturn orbit are very different to those at the Earth. The interplanetary magnetic field (IMF) strength and density drop by approximately 2 orders of magnitude and the Parker spiral angle increases from approximately 45° to approximately 86°, as discussed by *Jackman et al.* [2008]. The period of Cassini's orbital tour considered in this study occurred during the declining phase of the solar cycle. *Jackman et al.* [2004] examined the magnetic structure of the solar wind during Cassini's approach to the planet and found it to be dominated by alternate compressions and rarefactions, associated with the presence of corotating interaction regions in the solar wind.

[4] Other studies have aimed to reveal the nature of the magnetospheric obstacle itself. Contrary to the implications of the Pioneer and Voyager observations, *Arridge* [2007] and *Arridge et al.* [2008] demonstrated that the Cassini observations suggest the presence of a magnetodisc current sheet for all local times explored, and they showed that at these local times the current sheet is displaced northward of

[1]Space and Atmospheric Physics Group, The Blackett Laboratory, Imperial College London, London, UK.
[2]Atmospheric Physics Laboratory, Department of Physics and Astronomy, University College London, London, UK.
[3]Heliophysics Science Division, NASA GSFC, Greenbelt, Maryland, USA.
[4]Department of Physics and Astronomy, University of Iowa, Iowa City, Iowa, USA.
[5]Mullard Space Science Laboratory, Department of Space and Climate Physics, University College London, Dorking, UK.
[6]Centre for Planetary Sciences, University College London, London, UK.

Copyright 2008 by the American Geophysical Union.
0148-0227/08/2008JA013276

the magnetic dipole equator. They then argued that this is due to the stress balance corresponding to the solar wind impacting a magnetospheric obstacle which departs from symmetry about the plane containing the Saturn-Sun line ($\underline{x}$) and the vector $\underline{x} \times \underline{M}$, where $\underline{M}$ represents the planetary magnetic dipole vector. This deviation from symmetry is due to the orientation of the dipole vector $\underline{M}$ which is tilted at an angle of $\sim 20°$ in the antisunward direction.

[5] This Jovian-like magnetospheric configuration is also implied by the results of empirical modeling of the magnetopause. *Arridge et al.* [2006] used magnetopause crossings made by Voyager and Cassini to construct an empirical model of the surface and calculated that the magnetopause standoff distance varied in proportion to the solar wind dynamic pressure to the power $-1/4.3$. This is closer to the $-1/4$ value determined for Jupiter's magnetopause [*Huddleston et al.*, 1998] than the $-1/6$ value for the Earth. *Bunce et al.* [2007] argued that this increased compressibility arises because inertial stresses are important in the magnetodisc current sheet [*Arridge et al.*, 2007].

[6] The supermagnetosonic solar wind is deflected around this magnetospheric obstacle by the formation of a fast magnetosonic shock wave known as a bow shock (see the reviews by *Russell* [1985] and *Burgess* [1995]). This collisionless shock stands in the solar wind and plasma is slowed, heated and compressed as it crosses the shock. The submagnetosonic processed solar wind of the magnetosheath then flows around the magnetospheric cavity. Saturn's bow shock was first observed by Pioneer 11 in 1979 [*Acuña and Ness*, 1980] and the crossings made by Cassini during Saturn orbit insertion (SOI) were analyzed and discussed by *Achilleos et al.* [2006]. They found that the typical Mach number (ratio of upstream flow speed to the phase speed of a fast magnetosonic wave) was ~ 13 and estimated that the instantaneous velocity of the shock surface was of the order of 10 or 100 km s^{-1}. In addition, the length scales of the "ramp" and "foot" features of the bow shock indicated that the shock structure is governed by ion dynamics (e.g., reflection and gyration of solar wind ions back upstream [*Gosling and Robson*, 1985]).

[7] In this study we are interested in the global shape and location of Saturn's bow shock surface. Theoretically the shape of a shock wave due to a point object is given by a geometry known as the Mach cone, where the flaring angle is determined by the upstream Mach number. The global shape of planetary bow shocks is influenced in the far field by the Mach cone and in the near field by the geometry of the obstacle. Thus the dayside boundary is principally determined by the obstacle geometry [*Farris and Russell*, 1994], whereas downstream on the nightside the shape approaches the limit of the Mach cone [*Slavin et al.*, 1984].

1.1. Modeling Bow Shock Position and Shape

[8] General techniques used to empirically model planetary bow shock surfaces were reviewed by *Slavin and Holzer* [1981]. A functional form describing the geometry of the surface is chosen and the parameters that are a best fit to the observed spatial locations of the bow shock crossings are determined. To reduce the number of free parameters the surface is often assumed to be axially symmetric about the solar wind flow direction and the functional form of the model is chosen as a conic section.

$$r = \frac{L}{1 + \varepsilon \cos\theta}. \tag{1}$$

[9] The general equation of a conic section is given in equation (1), where r is the distance from the focus of the conic section to a point on the shock surface, θ is the corresponding polar coordinate angle with respect to the axis of symmetry, L is the semilatus rectum (size parameter), ε is the eccentricity and the focus position, x_0, is constrained to lie along the axis of symmetry. For $\varepsilon < 1$ the surface is ellipsoid, for $\varepsilon = 1$ the surface is paraboloid and for $\varepsilon > 1$ it is hyperboloid. Since the conic section is defined by the constants ε, L and x_0 the process of fitting a conic section to a given distribution of boundary crossings is a three parameter method, where these constants are taken as free parameters. Planetary bow shock surface models constructed using this functional form typically have a hyperbolic geometry (which corresponds to the most "blunt" geometry).

[10] Before calculating the best fit conic section it is often necessary to correct for two effects which influence the position of each shock crossing; the first of these is planetary orbital motion which determines the incident solar wind direction in the rest frame of the planet. For each crossing a planet-centered coordinate system is used where one axis is the planet-Sun line; the coordinate system is then rotated in the planet's orbital plane so that this axis becomes parallel to the solar wind flow direction. This is referred to as aberrated coordinates and the position of the crossing in this coordinate system is used in the construction of the model. At the Earth this involves a typical rotation of $\sim 3.8°$ [*Fairfield*, 1971] whereas at Saturn the typical rotation is by $\sim 1°$. The second correction is for the different values of the solar wind dynamic pressure which prevail at each observed boundary crossing. The location of the magnetopause is determined by a balance between the sum of the magnetic and plasma pressures inside the magnetopause and the solar wind dynamic pressure outside the magnetopause [*Petrinec and Russell*, 1993] (see the review by *Walker and Russell* [1995]), with increases in the solar wind dynamic pressure causing the magnetopause to contract whereas decreases cause it to expand. Since the bow shock is a consequence of the solar wind flow around the magnetopause the behavior of the shock surface with upstream solar wind dynamic pressure variations is similar. The power law shown in equation (2), which is defined by the constants c_1 and c_2, can be used to describe the relationship between bow shock standoff distance (R_{SN}; units: planetary radii) and solar wind dynamic pressure (P_{SW}; units: nPa).

$$R_{SN} = c_1 {P_{SW}}^{-1/c_2}. \tag{2}$$

[11] The standoff distance corresponds to the value of r given by equation (1) when $\theta = 0°$ and may be used as a proxy for the global size of the surface. To correct for solar wind dynamic pressure variations the aberrated position of each crossing is moved along the line that passes through a specified focal point (e.g., the center of the planet) and its

original position until its new position corresponds to the average dynamic pressure observed upstream of the entire set of crossings. The distance and direction that each aberrated crossing position is moved along the appropriate line is determined by the measured dynamic pressure upstream of the crossing and the power law. This approach assumes a self-similar scaling of the shock with dynamic pressure [*Binsack and Vasyliunas*, 1968] with the correction decreasing the spread of the crossing positions to provide an approximation to a bow shock surface at constant pressure. Once these two corrections have been made the best fit conic section to the resulting crossing position distribution is taken as an empirical model of the global bow shock surface and the power law predicts the scale of the surface for an arbitrary solar wind dynamic pressure.

[12] At the Earth, the large database of bow shock crossings compiled by orbiting spacecraft allows the terrestrial shock surface shape and location to be examined in detail (see the review by *Eastwood* [2003]). *Fairfield* [1971] demonstrated that the terrestrial bow shock orientation is aberrated as a result of planetary orbital motion and a number of other studies have investigated the global configuration of the shock and its dependence on various physical parameters [*Formisano*, 1979; *Slavin and Holzer*, 1981; *Farris et al.*, 1991; *Merka et al.*, 2005]. The bow shock surfaces of a number of other planets have been empirically modeled using similar techniques, although the corresponding databases of crossings are not as extensive [*Slavin et al.*, 1979, 1980; *Slavin and Holzer*, 1981; *Cairns et al.*, 1991; *Huddleston et al.*, 1998].

[13] Another technique for modeling planetary bow shocks based on observations was developed by *Khurana and Kivelson* [1994], who used a semi-empirical, semi-theoretical approach to model Venus' bow shock, which has also been used to model the Earth's distant bow shock [*Bennett et al.*, 1997]. The technique is based on empirical information and requires the surface to tend to the Mach cone predicted by MHD shock theory in the downstream limit. Both the size and shape of the shock surface are governed by upstream conditions and the predictions of the models were shown to be in good agreement with the locations of shock crossings made by spacecraft on the flanks of the cytherean and terrestrial bow shocks. This alternative technique is designed to model distant planetary bow shocks; in this study we aimed to model Saturn's dayside bow shock surface and so the general approach described in detail in this section has been preferred.

1.2. Existing Models of Saturn's Bow Shock

[14] The first existing model of Saturn's bow shock that is discussed in this study is the empirical model constructed by *Slavin et al.* [1985] which utilized the Pioneer and Voyager crossings. Prior to the Voyager 2 flyby an empirical model was also constructed by *Ness et al.* [1981]; however, since the *Slavin et al.* [1985] model also included the Voyager 2 crossings, combining all of the Pioneer and Voyager observations, we have considered the *Slavin et al.* [1985] model instead of the *Ness et al.* [1981] model.

[15] In the construction of their model, *Slavin et al.* [1985] averaged crossings that occurred within 10 h of each other to avoid biasing the model toward passes with a greater number of crossings; yielding a total of seven averaged crossings. By assuming an axially symmetric bow shock surface about the solar wind flow direction, and correcting the crossing positions as discussed in section 1.1, they constructed a model surface given by a conic section with an eccentricity of 1.71, a focus position at +6 R_S along the aberrated Saturn-Sun line (positive being toward the Sun), a size parameter (L) for the average shock location of 55.4 R_S and an associated power law of $R_{SN} = 13.33\ P_{SW}^{-1/5.1}$. In addition they used the same approach to construct an empirical conic section model for the magnetopause by assuming pressure balance to estimate the solar wind dynamic pressure associated with magnetopause crossings from measurements of the magnetospheric magnetic field. They found that the magnetopause standoff distance varied in proportion to the solar wind dynamic pressure to the power $-1/6.1$, suggesting a stiffer, more Earth-like magnetosphere. *Behannon et al.* [1983] discussed the possibility that Saturn's magnetosphere became immersed in Jupiter's magnetotail during the Voyager 2 flyby, which would imply that crossings made by Voyager 2 during its outbound pass correspond to conditions in the Jovian tail rather than the upstream solar wind. For such an interaction it is anticipated that the magnetosphere should undergo an unusually large expansion due to the low dynamic pressure in the Jovian tail relative to that in the solar wind [*Behannon et al.*, 1983]. However, only one of the seven averaged crossings used by *Slavin et al.* [1985] occurred during the Voyager 2 outbound pass yet did not correspond to the greatest distance from the center of the planet, this implies that interaction with the Jovian tail did not significantly bias their model.

[16] The second model of Saturn's bow shock was constructed by *Hendricks et al.* [2005] by building a bow shock surface around the magnetopause surface model of *Maurice et al.* [1996]. In its construction the relationship between bow shock standoff distance and the radius of curvature of the subsolar magnetopause of *Petrinec and Russell* [1997] was used and the surface was constrained to approach the Mach cone in the downstream limit. This theoretical model is well described by a conic section with an eccentricity of 1.02, focus position at the center of the planet and an associated power law of $R_{SN} = 13.17\ P_{SW}^{-1/5.8}$ [*Achilleos et al.*, 2006]. The model eccentricities reveal that the *Slavin et al.* [1985] model is considerably more flared than the *Hendricks et al.* [2005] model (which is close to a paraboloid).

[17] In this paper we present an empirical model of Saturn's bow shock surface based on Cassini observations that takes advantage of a far greater number of shock crossings than were available in the pre-Cassini era, thus providing a clearer picture of the global shock location and shape. The model is of importance to other studies that are concerned with the position of the bow shock, has implications for the nature of the solar wind flow around the Kronian magnetosphere and can be used to aid in understanding the local plasma environment in the vicinity of Titan as a function of solar wind dynamic pressure.

2. Observations

[18] The coordinate system utilized throughout this study is the Kronocentric Solar Magnetospheric (KSM) system which is Saturn-centered, with the positive x axis pointing

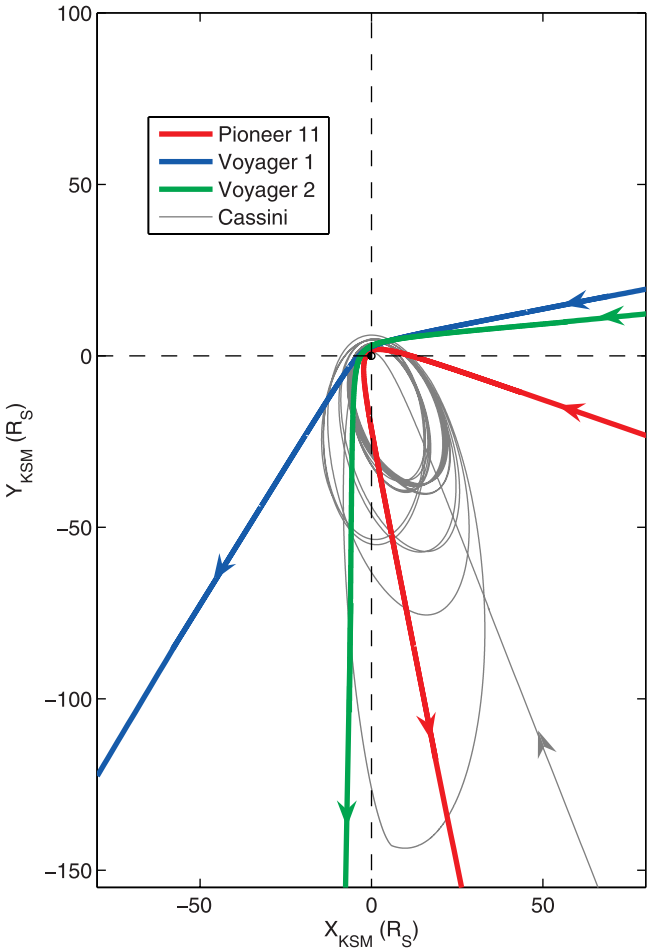

Figure 1. The trajectories of all the spacecraft that have explored the Kronian system projected into the *x-y* plane in Kronocentric Solar Magnetospheric (KSM) coordinates. Cassini's trajectory between June 2004 and August 2005 is shown.

toward the Sun and the *z* axis chosen such that the *x-z* plane contains Saturn's magnetic dipole axis with the positive *z* axis pointing north. The *y* axis completes the orthogonal set with the positive *y* axis pointing toward dusk. Since the angle between Saturn's magnetic dipole axis and spin axis is <1° [e.g., *Smith et al.*, 1980] the two axes have been assumed to be parallel in the construction of this coordinate system. The unit of distance used throughout this paper is Saturn radii (R_S; 1 R_S = 60268 km).

[19] Four spacecraft have visited the Kronian system to date; Pioneer 11 [*Acuña and Ness*, 1980], Voyager 1 [*Stone and Miner*, 1981] and Voyager 2 [*Stone and Miner*, 1982] flew by the planet in 1979, 1980 and 1981 respectively. The Cassini spacecraft arrived at Saturn in June 2004 and is the first Saturn orbiter [*Matson et al.*, 2002]; Cassini's prime orbital tour will last until mid-2008 and will be extended. The projection of the trajectories of all four spacecraft into the *x-y* plane is shown in Figure 1. The inbound passes of the Pioneer and Voyager spacecraft took place in the subsolar region, with Pioneer 11 and Voyager 2 leaving the magnetosphere close to the dawn meridian and Voyager 1 exiting further downtail, also in the dawn sector. Cassini's trajectory is shown from SOI (June 2004) until August 2005, during this phase of the orbital tour the spacecraft explored the dawnside magnetosphere at low latitudes. Crossings of the bow shock were made by all of these spacecraft; later in this section the precise positions of the combined set of crossings will be discussed. We only considered the Cassini crossings that occurred before 15 August 2005 because at the start of this study some of the data sets required to carry out our analysis were unavailable past this date. At the end of Cassini's orbital tour of the Saturn system it will be possible to construct a model of the bow shock using a far more extensive set of crossings.

[20] To identify the Cassini bow shock crossings during the period considered, data taken by two instruments mounted on the orbiter were used. The dual-technique magnetometer (MAG) consists of a fluxgate and a vector helium magnetometer; we have used 1s resolution magnetic field vector measurements made by the fluxgate magnetometer [*Dougherty et al.*, 2004]. Data obtained by the electron spectrometer sensor (ELS) of the Cassini plasma spectrometer (CAPS) instrument suite were also used in the identification [*Young et al.*, 2004]. In the construction of the model, data taken by the Radio and Plasma Wave System (RPWS) were used [*Gurnett et al.*, 2004]. RPWS is able to measure electron number densities from observations of the Langmuir wave frequency; to construct the model these measurements were essential.

[21] We began by identifying bow shock crossings in the Cassini magnetic field and electron data and combined these with those made by Pioneer 11, Voyager 1, and Voyager 2 [*Acuña and Ness*, 1980; *Bridge et al.*, 1981, 1982; *Ness et al.*, 1981, 1982]. The MAG and ELS observations of the first crossing made by Cassini during its initial approach to the planet in June 2004 are shown in Figure 2; the time-energy spectrogram of electron counts is from ELS anode 5. There is a clear increase in the strength and variability of the field as the shock is crossed and spacecraft photoelectrons are observed throughout the interval below 10 eV. Downstream of the shock the hotter, denser magnetosheath electron population is evident whereas upstream of the shock the solar wind electron distribution is obscured by the spacecraft photoelectrons [*Ishisaka et al.*, 2001; *Young et al.*, 2005; *Masters et al.*, 2008]. This clear upstream to downstream transition is typical of the signatures of the crossings seen by all of the spacecraft; however, for a number of the Cassini crossings there was a more disturbed magnetic and plasma transition which prohibited the precise determination of the shock crossing location. The change in the position of the spacecraft from the beginning to the end of these transitions was negligible relative to the scale of the global shock surface that we were aiming to empirically model, as a result we were able to include such crossings by taking the central time of each transition as the crossing time. These two categories of magnetic and plasma signature are due to different shock geometries, a discussion of which is beyond the scope of this paper (see the reviews by *Bale et al.* [2005] and *Burgess et al.* [2005]).

[22] A list of all the Cassini bow shock crossings identified in the interval considered is given in Table 1. The total crossing set was then composed of the identified Cassini

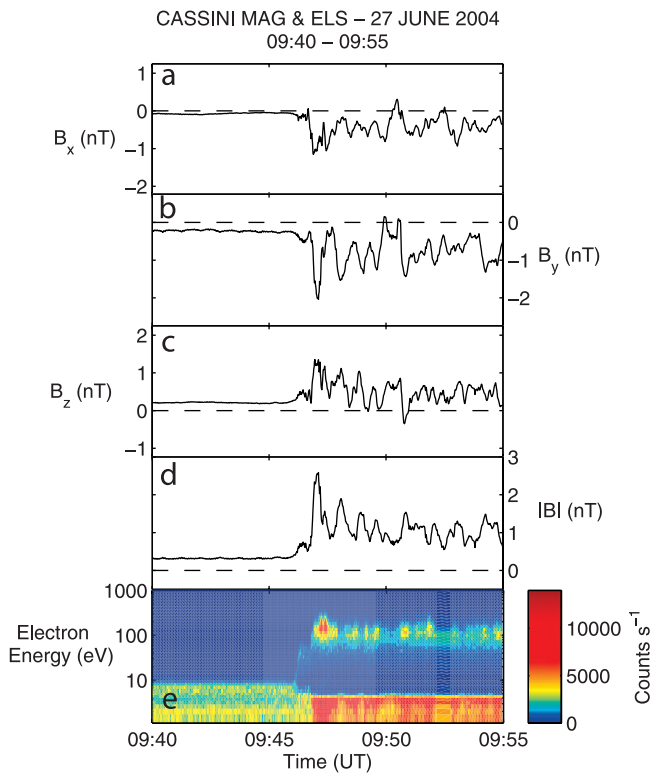

Figure 2. Dual-technique magnetometer (MAG) and electron spectrometer sensor (ELS) data for a 15-min interval surrounding the first crossing of Saturn's bow shock made by Cassini. (a–c) The components of the magnetic field in KSM coordinates. (d) The field magnitude. (e) A time-energy spectrogram of electron counts from ELS anode 5.

crossings and the Pioneer and Voyager crossings, at which stage a number of the crossings made by Voyager 1 and 2 were omitted from further consideration for the following reasons. During the outbound pass of Voyager 1 a single crossing was made at an x coordinate of ~ -40.0 R_S, whereas all other crossings occurred at x coordinates greater than ~ -10.0 R_S. As a result we were able to study the region of the shock surface where the boundary location and shape is principally determined by the geometry of the magnetospheric obstacle. Since the Voyager 1 outbound crossing was the only crossing that occurred downtail, where the shock location is principally determined by the geometry of the Mach cone instead, it was removed from the set of crossings. We note that the lack of bow shock crossings in the downstream limit implies that the model constructed in section 3 cannot be used to infer the upstream fast magnetosonic Mach number [*Slavin et al.*, 1984]. We have also omitted the crossings made during the outbound pass of Voyager 2 as there is a possibility that they correspond to the Jovian magnetotail, rather than solar wind, interaction with the magnetosphere [*Behannon et al.*, 1983]. The positions of the crossings in the final set, following these exclusions, are shown in Figure 3. The total number of crossings is 217; they occurred at latitudes between $-22.4°$ and $17.9°$ and between local times of 0524 and 1318. Principally owing to solar wind dynamic pressure variations the spread in the crossing positions is considerable, and a clear outline of the shock surface is not immediately evident.

[23] The final comment to make regarding the positions of the shock crossings concerns the spacecraft trajectories. The bow shock moves at a speed much greater than that of any of the spacecraft and as a result, for a given pass, multiple crossings are typically observed owing to the quasi-oscillatory motion of the shock. Figure 3 shows some clear examples of such sets of multiple crossings. In addition, for a number of the Cassini orbits the point of apoapsis of the orbit led to the spacecraft moving approximately parallel to the shock surface in a region of space where the shock is typically observed. Consequently for these orbits a larger number of crossings occurred; this is also evident in Figure 3.

3. Model Construction

[24] In order to investigate the location and shape of the shock surface it is essential to correct for variations in the solar wind dynamic pressure. For the Cassini bow shock crossings the CAPS instrument was not able to measure the properties of the solar wind plasma flow upstream of each crossing owing to pointing constraints; this prohibited direct measurements of the dynamic pressure. Since our total crossing set is heavily dominated by Cassini crossings we made a number of assumptions in order to overcome this problem; in this section we detail those assumptions and then present the new model itself. In section 4.1 the validity of the assumptions described here will be tested in order to justify the new model.

3.1. Assumptions

[25] In the absence of solar wind dynamic pressure measurements upstream of the Cassini crossings we have used estimates. The dynamic pressure is given by $\rho_m v_{sw}^2$, where ρ_m is the plasma mass density and v_{sw} is the plasma flow speed. Although pointing constraints prohibited CAPS observations of the solar wind plasma flow upstream of the Cassini crossings, such observations were made between 10 and 30 January 2004 during Cassini's approach to the planet. During this period measurements of the solar wind flow were made by the CAPS instrument while the Hubble Space Telescope observed Saturn's ultraviolet aurorae. *Crary et al.* [2005] presented and analyzed these data to investigate the factors controlling the Kronian aurorae and presented measurements of solar wind proton number density and flow speed. Proton number densities were in the range $\sim$0.002 to $\sim$0.4 cm^{-3} and flow speeds were in the range $\sim$430 to $\sim$620 km s^{-1}. The range of each parameter indicates a highly variable dynamic pressure as anticipated.

[26] To estimate the dynamic pressure upstream of each Cassini bow shock crossing we used upstream RPWS measurements of the electron number density. By then assuming a charge-neutral solar wind plasma composed of 4% doubly ionized helium by number we obtained the plasma mass density (ρ_m), and by this approach we calculated proton number densities in the range 0.0067 to 0.38 cm^{-3}. This range is in good agreement with the range of the CAPS measurements presented by *Crary et al.* [2005]; this provides some justification for the use of RPWS

Table 1. List of Times and Locations of Cassini Bow Shock Crossings Between 1 June 2004 and 15 August 2005

Crossing	Year	Month	Day of Month	Day of Year	Time (UT)	X_{KSM}	Y_{KSM}	Z_{KSM}
1	2004	Jun	27	179	0946	22.4	−43.5	−4.4
2	2004	Jun	27	179	1028	22.3	−43.2	−4.3
3	2004	Jun	27	179	1804	21.1	−40.2	−3.8
4	2004	Jun	27	179	2000	20.8	−39.4	−3.7
5	2004	Jun	28	180	0018	20.1	−37.6	−3.4
6	2004	Jun	28	180	0257	19.6	−36.5	−3.3
7	2004	Jun	28	180	0538	19.3	−35.6	−3.1
8	2004	Jul	7	189	1405	−8.1	−50.9	−21.3
9	2004	Jul	7	189	1615	−8.1	−51.4	−21.4
10	2004	Jul	7	189	2146	−8.0	−52.6	−21.8
11	2004	Jul	8	190	0030	−8.0	−53.1	−22.0
12	2004	Jul	8	190	0413	−8.0	−53.9	−22.3
13	2004	Jul	8	190	1056	−7.9	−55.3	−22.7
14	2004	Jul	8	190	1154	−7.9	−55.5	−22.8
15	2004	Jul	12	194	0512	−7.1	−71.5	−27.8
16	2004	Jul	14	196	0311	−6.5	−78.5	−30.0
17	2004	Jul	14	196	0659	−6.5	−79.1	−30.2
18	2004	Oct	25	299	0615	22.7	−18.7	6.6
19	2004	Oct	25	299	0648	22.7	−18.6	6.6
20	2004	Oct	25	299	1222	21.9	−16.8	6.8
21	2004	Nov	4	309	2241	−7.5	−47.5	−16.5
22	2004	Nov	5	310	0334	−7.2	−48.3	−16.5
23	2004	Nov	5	310	1336	−6.6	−50.0	−16.6
24	2004	Nov	5	310	1733	−6.4	−50.7	−16.7
25	2004	Nov	6	311	0441	−5.6	−52.4	−16.7
26	2004	Nov	6	311	0744	−5.4	−52.9	−16.7
27	2004	Nov	6	311	1436	−5.0	−53.9	−16.8
28	2004	Nov	6	311	2301	−4.4	−55.1	−16.8
29	2004	Nov	7	312	1243	−3.5	−57.0	−16.8
30	2004	Dec	10	345	0907	25.7	−29.2	6.4
31	2004	Dec	10	345	1020	25.6	−28.9	6.4
32	2004	Dec	10	345	1324	25.4	−28.1	6.5
33	2004	Dec	10	345	1518	25.3	−27.7	6.5
34	2004	Dec	10	345	1546	25.2	−27.6	6.5
35	2004	Dec	10	345	1817	25.1	−26.9	6.6
36	2004	Dec	11	346	2336	22.5	−19.2	7.2
37	2004	Dec	12	347	0403	22.0	−17.9	7.3
38	2004	Dec	12	347	0742	21.5	−16.8	7.3
39	2004	Dec	23	358	2037	4.8	−50.5	−2.6
40	2004	Dec	24	359	0923	5.9	−51.7	−2.2
41	2004	Dec	25	360	0445	7.5	−53.3	−1.6
42	2004	Dec	26	361	0114	9.3	−54.6	−0.9
43	2004	Dec	26	361	0126	9.3	−54.6	−0.9
44	2005	Jan	3	003	1904	22.8	−52.7	5.5
45	2005	Jan	4	004	0234	23.2	−52.2	5.7
46	2005	Jan	4	004	0548	23.3	−51.9	5.8
47	2005	Jan	4	004	2136	23.9	−50.6	6.2
48	2005	Jan	24	024	0301	1.5	−48.5	−3.8
49	2005	Jan	24	024	0655	1.8	−48.9	−3.7
50	2005	Jan	24	024	1422	2.4	−49.8	−3.5
51	2005	Jan	27	027	1601	8.5	−55.4	−1.2
52	2005	Jan	27	027	1613	8.6	−55.4	−1.2
53	2005	Feb	11	042	0752	24.4	−32.6	8.1
54	2005	Feb	11	042	0822	24.4	−32.6	8.1
55	2005	Feb	11	042	1930	24.1	−30.3	8.2
56	2005	Feb	24	055	0846	12.8	−39.5	5.3
57	2005	Mar	1	060	0731	21.6	−36.2	8.9
58	2005	Mar	1	060	1606	22.0	−35.5	9.0
59	2005	Mar	4	063	1607	22.8	−25.7	9.3
60	2005	Mar	5	064	1640	21.9	−20.9	8.9
61	2005	Mar	5	064	1640	21.9	−20.8	8.9
62	2005	Mar	5	064	1839	21.8	−20.5	8.9
63	2005	Mar	14	073	1925	7.3	−36.4	3.0
64	2005	Mar	14	073	2240	7.6	−36.8	3.1
65	2005	Mar	14	073	2347	7.8	−36.9	3.2
66	2005	Mar	15	074	0001	7.8	−36.9	3.2
67	2005	Mar	15	074	0050	7.9	−37.0	3.2
68	2005	Mar	15	074	0242	8.1	−37.1	3.3
69	2005	Mar	15	074	0319	8.2	−37.2	3.3
70	2005	Mar	15	074	0346	8.2	−37.2	3.4
71	2005	Mar	15	074	0538	8.4	−37.4	3.4
72	2005	Mar	15	074	0711	8.6	−37.5	3.5
73	2005	Mar	15	074	1017	9.0	−37.8	3.7

Table 1. (continued)

Crossing	Year	Month	Day of Month	Day of Year	Time (UT)	X_{KSM}	Y_{KSM}	Z_{KSM}
74	2005	Mar	15	074	1201	9.2	−37.9	3.7
75	2005	Mar	15	074	1512	9.5	−38.2	3.9
76	2005	Mar	16	075	0229	10.7	−38.9	4.4
77	2005	Mar	16	075	0249	10.8	−38.9	4.4
78	2005	Mar	16	075	2207	12.7	−39.8	5.2
79	2005	Mar	17	076	0153	13.1	−40.0	5.3
80	2005	Mar	17	076	0831	13.7	−40.1	5.6
81	2005	Mar	18	077	2308	17.1	−40.2	7.0
82	2005	Mar	19	078	0235	17.4	−40.1	7.1
83	2005	Mar	19	078	0821	17.8	−40.0	7.2
84	2005	Mar	20	079	0211	19.1	−39.3	7.7
85	2005	Mar	20	079	0817	19.5	−39.0	7.9
86	2005	Mar	20	079	0920	19.5	−38.9	7.9
87	2005	Mar	20	079	1440	19.8	−38.6	8.1
88	2005	Mar	20	079	1723	20.0	−38.5	8.1
89	2005	Mar	25	084	0519	22.6	−25.7	9.1
90	2005	Mar	25	084	1333	22.4	−24.2	9.0
91	2005	Mar	27	086	0015	20.4	−16.7	8.2
92	2005	Mar	27	086	0236	20.2	−16.1	8.1
93	2005	Mar	27	086	0526	19.9	−15.4	8.0
94	2005	Mar	27	086	0702	19.7	−15.0	8.0
95	2005	Mar	27	086	0903	19.5	−14.5	7.9
96	2005	Apr	12	102	0016	16.2	−21.4	3.8
97	2005	Apr	12	102	0240	16.1	−20.8	3.7
98	2005	Apr	12	102	1038	15.8	−18.9	3.7
99	2005	Apr	12	102	1531	15.6	−17.6	3.7
100	2005	Apr	12	102	2115	15.2	−16.0	3.6
101	2005	Apr	12	102	2207	15.1	−15.7	3.6
102	2005	Apr	13	103	0027	14.9	−15.0	3.5
103	2005	Apr	13	103	0109	14.8	−14.8	3.5
104	2005	Apr	20	110	1839	9.4	−35.9	−2.3
105	2005	Apr	20	110	1900	9.4	−35.9	−2.3
106	2005	Apr	21	111	0125	10.2	−36.3	−2.3
107	2005	Apr	21	111	0847	11.0	−36.7	−2.3
108	2005	Apr	21	111	1046	11.3	−36.7	−2.3
109	2005	Apr	24	114	0422	17.7	−36.5	−2.3
110	2005	Apr	24	114	0543	17.9	−36.4	−2.3
111	2005	Apr	24	114	0828	18.1	−36.3	−2.3
112	2005	Apr	24	114	1247	18.4	−36.0	−2.2
113	2005	Apr	24	114	2152	19.1	−35.5	−2.2
114	2005	Apr	26	116	0809	21.1	−32.5	−2.0
115	2005	Apr	26	116	1010	21.2	−32.3	−2.0
116	2005	May	10	130	2051	14.0	−37.4	−2.5
117	2005	May	10	130	2126	14.1	−37.4	−2.5
118	2005	May	11	131	0046	14.4	−37.4	−2.5
119	2005	May	14	134	0542	20.4	−33.4	−2.2
120	2005	May	16	136	0155	21.9	−27.7	−1.9
121	2005	May	16	136	0601	21.9	−27.1	−1.8
122	2005	May	16	136	1025	22.0	−26.3	−1.8
123	2005	May	16	136	1437	22.0	−25.6	−1.7
124	2005	May	16	136	1522	22.0	−25.5	−1.7
125	2005	May	16	136	1543	22.0	−25.4	−1.7
126	2005	May	28	148	1229	12.3	−37.4	−2.7
127	2005	May	28	148	1251	12.4	−37.5	−2.7
128	2005	May	28	148	1637	12.8	−37.5	−2.7
129	2005	Jun	1	152	1614	20.4	−32.9	−2.4
130	2005	Jun	1	152	1706	20.4	−32.8	−2.4
131	2005	Jun	1	152	1941	20.6	−32.6	−2.4
132	2005	Jun	1	152	2143	20.7	−32.3	−2.4
133	2005	Jun	2	153	0110	20.8	−31.9	−2.4
134	2005	Jun	2	153	0457	21.0	−31.5	−2.3
135	2005	Jun	2	153	1833	21.4	−29.7	−2.2
136	2005	Jun	2	153	2020	21.5	−29.4	−2.2
137	2005	Jun	3	154	1104	21.7	−27.2	−2.0
138	2005	Jun	3	154	2046	21.7	−25.5	−1.9
139	2005	Jun	3	154	2132	21.7	−25.4	−1.9
140	2005	Jun	4	155	0301	21.7	−24.4	−1.8
141	2005	Jun	4	155	0324	21.7	−24.3	−1.8
142	2005	Jun	4	155	0602	21.7	−23.8	−1.8
143	2005	Jun	4	155	0849	21.6	−23.3	−1.7
144	2005	Jun	4	155	1043	21.6	−22.9	−1.7
145	2005	Jun	4	155	1838	21.3	−21.2	−1.6
146	2005	Jun	4	155	2041	21.3	−20.8	−1.6

Table 1. (continued)

Crossing	Year	Month	Day of Month	Day of Year	Time (UT)	X_{KSM}	Y_{KSM}	Z_{KSM}
147	2005	Jun	4	155	2345	21.1	−20.1	−1.5
148	2005	Jun	20	171	0809	20.6	−31.9	−2.6
149	2005	Jun	20	171	1340	20.9	−31.2	−2.6
150	2005	Jun	20	171	1706	21.0	−30.7	−2.5
151	2005	Jun	21	172	1421	21.5	−27.6	−2.3
152	2005	Jun	21	172	1754	21.5	−27.1	−2.2
153	2005	Jun	22	173	0900	21.5	−24.4	−2.0
154	2005	Jun	22	173	1205	21.5	−23.8	−2.0
155	2005	Jun	23	174	0532	21.0	−20.1	−1.7
156	2005	Jun	23	174	0633	20.9	−19.9	−1.7
157	2005	Jun	23	174	1224	20.6	−18.5	−1.5
158	2005	Jun	23	174	1411	20.5	−18.1	−1.5
159	2005	Jun	23	174	1729	20.3	−17.3	−1.4
160	2005	Jun	23	174	1957	20.1	−16.7	−1.4
161	2005	Jun	23	174	2345	19.8	−15.7	−1.3
162	2005	Jun	24	175	0609	19.2	−14.0	−1.2
163	2005	Jun	24	175	0721	19.1	−13.7	−1.2
164	2005	Jul	1	182	1048	4.6	−33.9	−2.9
165	2005	Jul	1	182	1523	5.2	−34.4	−3.0
166	2005	Jul	1	182	1847	5.6	−34.7	−3.0
167	2005	Jul	1	182	2043	5.9	−34.9	−3.0
168	2005	Jul	2	183	0511	6.9	−35.7	−3.1
169	2005	Jul	2	183	0939	7.5	−36.0	−3.1
170	2005	Jul	2	183	1719	8.4	−36.5	−3.2
171	2005	Jul	2	183	2020	8.7	−36.7	−3.2
172	2005	Jul	3	184	1439	10.8	−37.5	−3.3
173	2005	Jul	3	184	1735	11.1	−37.6	−3.3
174	2005	Jul	3	184	1822	11.2	−37.6	−3.3
175	2005	Jul	3	184	2203	11.6	−37.7	−3.3
176	2005	Jul	4	185	0005	11.8	−37.8	−3.3
177	2005	Jul	4	185	1800	13.7	−37.9	−3.3
178	2005	Jul	6	187	1613	17.7	−36.3	−3.2
179	2005	Jul	6	187	1925	17.9	−36.1	−3.2
180	2005	Jul	7	188	1434	19.2	−34.6	−3.1
181	2005	Jul	7	188	1457	19.2	−34.5	−3.1
182	2005	Jul	7	188	1853	19.4	−34.2	−3.0
183	2005	Jul	7	188	2209	19.6	−33.9	−3.0
184	2005	Jul	7	188	2218	19.6	−33.9	−3.0
185	2005	Jul	7	188	2248	19.6	−33.8	−3.0
186	2005	Jul	11	192	0533	21.0	−21.7	−2.0
187	2005	Jul	11	192	1114	20.8	−20.5	−1.9
188	2005	Jul	11	192	1502	20.7	−19.6	−1.8
189	2005	Jul	11	192	1834	20.5	−18.8	−1.7
190	2005	Jul	12	193	0910	19.4	−15.1	−1.4
191	2005	Jul	12	193	1543	18.8	−13.3	−1.2
192	2005	Jul	24	205	1813	17.0	−36.8	−3.5
193	2005	Jul	28	209	2213	21.1	−24.9	−2.4
194	2005	Jul	28	209	2352	21.1	−24.6	−2.4
195	2005	Jul	29	210	1548	20.8	−21.3	−2.1
196	2005	Jul	29	210	2037	20.6	−20.3	−2.0
197	2005	Aug	8	220	2258	9.5	−37.4	−3.7
198	2005	Aug	9	221	0023	9.6	−37.5	−3.7
199	2005	Aug	9	221	0123	9.7	−37.5	−3.7
200	2005	Aug	9	221	2129	11.9	−38.0	−3.8
201	2005	Aug	10	222	0345	12.5	−38.0	−3.8
202	2005	Aug	11	223	0046	14.5	−37.8	−3.8
203	2005	Aug	11	223	0314	14.7	−37.7	−3.8
204	2005	Aug	11	223	0630	15.0	−37.6	−3.8
205	2005	Aug	11	223	1815	16.0	−37.2	−3.7
206	2005	Aug	12	224	1331	17.5	−36.0	−3.7

observations to calculate solar wind mass densities. The main assumption made in the construction of the model was that the solar wind flow speed (v_{sw}) was equal to (500 ± 100) km s^{-1} upstream of all the Cassini crossings; this assumed value was based on the measurements presented by *Crary et al.* [2005]. The solar wind dynamic pressure upstream of each Cassini crossing was then estimated, with the 20% relative error in v_{sw} resulted in a relative error of ~40% in each estimate.

[27] We required that the RPWS measurements were made within approximately 7 min upstream of each shock crossing. This was an arbitrary choice of interval length that was used to identify density measurements close to the time of each shock crossing. For a number of the Cassini crossings the Langmuir frequency was not well resolved in this interval and thus these crossings have not been used in the construction of the model. Generally, RPWS density measurements were either available in this interval or else the

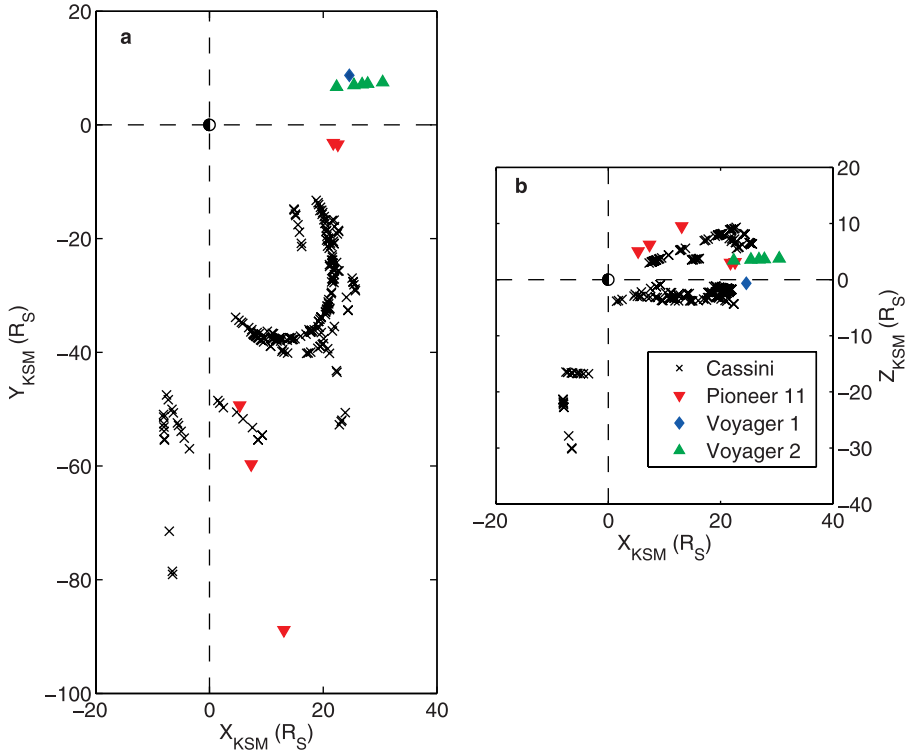

Figure 3. The positions of the bow shock crossings considered in this study. (a) The positions projected into the *x*-*y* plane in KSM coordinates. (b) The positions projected into the *x*-*z* plane in KSM coordinates. The crossings made by each spacecraft are indicated.

most recent upstream measurement was made at a time greater than approximately 1 hour before or after the crossing; such a measurement is not necessarily representative of the solar wind mass density at the time of the crossing in question. Thus the results presented and discussed in this paper were not sensitive to changes in the length of this interval. Figure 4 shows the positions of the 163 crossings used in the construction of the model; this set is the combination of the Cassini crossings associated with RPWS densities and the Pioneer and Voyager crossings. For the Pioneer and Voyager crossings upstream measurements of the solar wind speed and density were made and thus we were able to use direct measurements of the solar wind dynamic pressure rather than estimates. The range of these measurements was 0.0076 to 0.12 nPa and the average was (0.05 ± 0.01) nPa, whereas the range of the Cassini dynamic pressure estimates was 0.0033 to 0.19 nPa with an average of (0.048 ± 0.003) nPa. Since the averages of the estimated and measured pressures are within errors, and their ranges are similar, we conclude that the solar wind dynamic pressure measurements and estimates are statistically consistent.

[28] Given the distribution of the crossings shown in Figure 4 we were able to construct an empirical model of the dawnside, low-latitude bow shock. Owing to the crossing coverage, we assumed that the surface was axially symmetric about the solar wind flow direction, which enabled us to consider the crossing positions in two rather than three coordinates by replacing the *y* and *z* coordinates with the ρ coordinate (the perpendicular distance from the *x* axis). To correct for Saturn's orbital motion we transformed the crossing positions into aberrated coordinates using measured solar wind velocities for the Pioneer and Voyager crossings and the assumed antisunward velocity of 500 km s^{-1} for the Cassini crossings. The resulting rotation in Saturn's orbital plane was ~1°; Saturn's orbital motion does not have a large effect on bow shock location compared to the case for the Earth [*Fairfield*, 1971]. Aberrated coordinates are denoted by prime symbols (x', ρ'), and the positions of the crossings in this coordinate system are shown in Figure 5. The best fit conic section was calculated using a nonlinear least squares technique where the focus was fixed at the center of the planet and the root mean square (RMS) of the perpendicular distance of the data points from the conic section was minimized. For the best fit to the distribution shown in Figure 5 this RMS normal deviation is 5.38 R_S; the global shape of the shock surface is not clear in Figure 5. Throughout this study whenever a best fit conic section was calculated the effect of outlying data points was considered. Five random subsamples of the data were used by choosing 50% of the data points randomly with replacement. By calculating the best fit to each subsample we obtained a distribution of each conic section parameter. For all the fits presented in this paper there was a variation of less than 5% in each parameter and thus none of the best fits were sensitive to outlying data points.

[29] To construct a power law relating bow shock standoff distance to solar wind dynamic pressure we used this initial conic section and changed the size parameter (*L*) to scale the conic section so that it intersected each crossing position, allowing the standoff distance to be projected in each case. To investigate the power law relationship, the solar wind dynamic pressures (estimates and measurements)

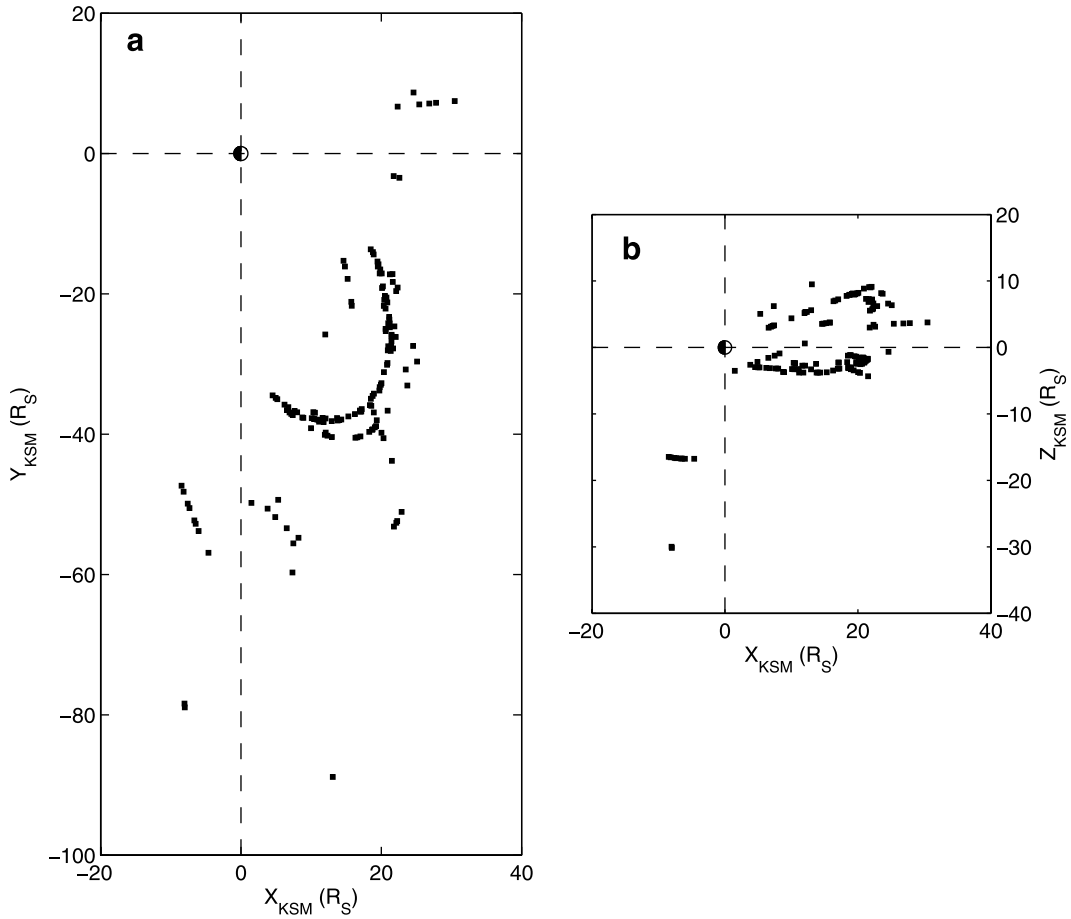

Figure 4. The positions of the bow shock crossings used in the construction of the model. (a) The positions projected into the *x*-*y* plane in KSM coordinates. (b) The positions projected into the *x*-*z* plane in KSM coordinates.

were plotted against the projected standoff distances on a logarithmic scale. Calculating the line of best fit of the distribution using a linear least squares technique allowed the determination of the constants c_1 and c_2 that define the power law. This plot and the power law are shown in Figure 6; there is a large relative error in the power law constant c_2 which is determined as (6 ± 2). The main source of this large error is our assumed solar wind speed of (500 ± 100) km s^{-1} upstream of all the Cassini crossings which results in a relative error of ~40% in each Cassini crossing dynamic pressure estimate. Since the c_2 constant defines the compressibility of the bow shock surface with changes in dynamic pressure, the extent of the compressibility of the bow shock surface cannot be accurately constrained.

[30] There are also other sources of the large error associated with c_2, for example the position of the shock is also influenced by the fast magnetosonic Mach number. As we have not been able to take into account the variation of this parameter this also contributes to the error. An important point to note is that the *Arridge et al.* [2006] model of Saturn's magnetopause has a dynamic pressure-dependent shape. For increasing dynamic pressure the magnetopause flaring decreases and vice versa. In this study we have used a set of self-similar conic sections to model the bow shock which constrains the shock surface to have a constant shape. The effect of the changing shape of the magnetopause obstacle is not taken into account by this approach and represents another source of the large error in the power law constant c_2.

[31] As the bow shock is a consequence of the magnetopause obstacle the response of the bow shock to dynamic pressure changes is intimately related to that of the magnetopause. The empirical modeling of *Arridge et al.* [2006] concluded that the response of Saturn's magnetopause can be described by a power law with c_2 = (4.3 ± 0.3). Since this value is within errors of the value we calculated for the bow shock, has a considerably smaller relative error and we expect the response of the two boundaries to be similar, we assumed that the value of c_2 in the bow shock power law was also equal to 4.3. This assumption is that the scaling of the bow shock with dynamic pressure variations is identical to that of the magnetopause.

[32] Our final assumption was that spacecraft trajectory effects would not bias an empirical model of the bow shock. Owing to spacecraft speeds less than that of the shock surface up to 10 crossings were observed in a typical pass, this is ~7% of our total number of crossings; since such crossing sets occur at a range of local times this effect does not introduce a significant bias. However, the majority of the crossings occurred between local times of ~0630 and

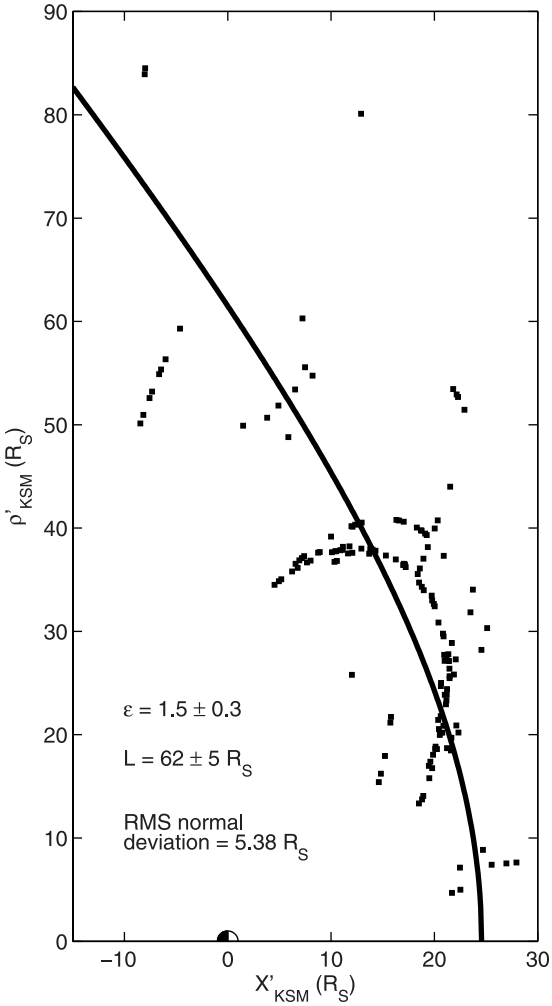

Figure 5. The positions of the bow shock crossings used in the construction of the model projected into the aberrated x-ρ plane. The best fit conic section is shown as a black curve, and its parameters are given.

~0940 owing to the location of the point of apoapsis of certain Cassini orbits, as discussed in section 2. Different approaches to removing this bias have been outlined in other studies of planetary bow shocks, for example *Formisano* [1979] considered crossings of the Earth's bow shock and divided the total spatial extent in which the crossings occurred into cubes of side one Earth radius. They then attached a statistical weight to each crossing on the basis of the amount of time that the spacecraft in question spent in the cube in which the crossing took place. Another approach was taken by *Slavin and Holzer* [1981], who tackled the problem by excluding crossings made during spacecraft orbits where the point of apoapsis was near the mean location of the shock, as well as statistically weighting crossings from orbits that were close to fulfilling the exclusion criterion. In this study we assume that our model of Saturn's bow shock is not biased by this effect.

3.2. Model

[33] After making these assumptions the correction for solar wind dynamic pressure variation was made using the assumed value of the power law constant c_2. The aberrated crossing positions were scaled to the average dynamic pressure of 0.048 nPa about the center of the planet, resulting in the pressure-corrected distribution shown in Figure 7. This correction decreased the spread of the crossing distribution and made the global shape of the shock surface clearer as expected. The best fit conic section to the pressure-corrected crossing positions was calculated using a nonlinear least squares technique, where the focus was fixed at the center of the planet and the RMS of the perpendicular distance of the data points from the conic section was minimized. We present this best fit conic section after the pressure correction as the new empirical model of Saturn's bow shock.

[34] The new model conic section is shown in Figure 7; the decrease in the spread of the distribution is quantified by the RMS normal deviation of the crossing positions to the conic section of 3.43 R_S which is less than the value of 5.38 R_S corresponding to the best fit before the pressure correction. In addition the model RMS normal deviation of 3.43 R_S is comparable to the value of 3.6 R_S associated with the *Slavin et al.* [1985] conic section model of Saturn's bow shock, which was constructed using a similar approach. This implies that, despite the large errors in the Cassini solar wind dynamic pressure estimates, the pressure correction reveals the location and shape of the shock surface to a greater extent than the existing empirical model. The best fit conic section to the crossing distribution before the pressure correction is also shown in Figure 7 for comparison and illustrates that the new model is more streamlined, with an eccentricity of (1.05 ± 0.09), this implies a marginally hyperbolic geometry. Using the new model conic section the value of the power law constant c_1 was calculated as (12.3 ± 0.7) R_S to complete the new empirical model which is described by equations (3) and (4):

$$r = \frac{L}{1 + 1.05\cos\theta}, \tag{3}$$

$$R_{SN} = 12.3 P_{SW}{}^{-1/4.3} = \frac{L}{2.05}, \tag{4}$$

where equation (3) yields the new model surface and equation (4) shows the corresponding power law, with its assumed value of c_2 = 4.3. Using the power law the size parameter of the model conic section for a given solar wind dynamic pressure can be calculated as shown in equation (4), this allows the location of the shock to be predicted for an arbitrary solar wind dynamic pressure. The size parameter of the average shock location shown in Figure 7 is (51 ± 2) R_S, which implies that the average shock standoff distance is (25 ± 1) R_S, The dependence of the global configuration of the shock on the orientation of the IMF was also considered, however no clear relationship was found.

[35] The variability of the bow shock standoff distance can be examined in two ways. First, the power law shown in equation (4) can be used to calculate the standoff distance for each crossing using its corresponding dynamic pressure. Second, the new model conic section given by equation (3) (and shown in Figure 7) can be scaled by varying its size

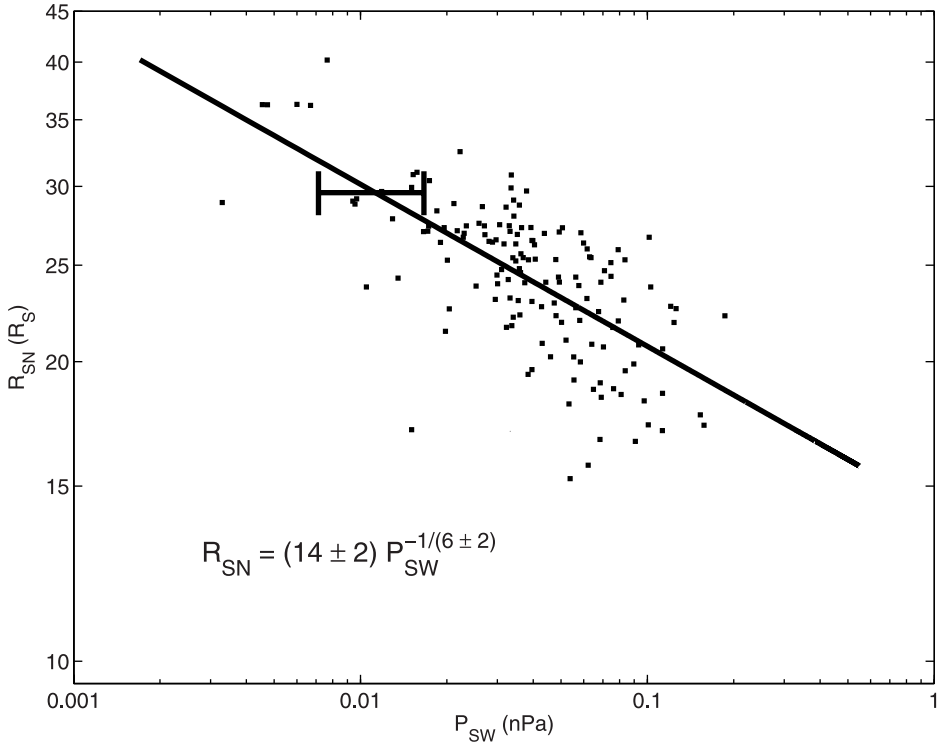

Figure 6. The plot of projected bow shock standoff distance (R_{SN}) against solar wind dynamic pressure (P_{SW}) on a logarithmic scale. The line of best fit is shown as a black line, and the corresponding power law relation is given. An error bar is plotted on one point that is typical of all the points.

parameter (L) so that it intersects each crossing position shown in Figure 5, projecting the standoff distance in each case. Using either approach the bow shock standoff distance is inferred to range from ~18 to ~46 R_S. In the crossing distribution before the pressure correction shown in Figure 5 there are a limited number of crossings in the subsolar region, all of which were made by the Pioneer and Voyager spacecraft. The positions of these crossings imply that their associated standoff distances lie between ~20 and ~30 R_S, considerably lower than the predicted maximum of ~46 R_S. However, this is not conclusive evidence that such large standoff distances do not occur since we have a limited number of observations near the subsolar point and the solar wind conditions required to produce such standoff distances are expected to be relatively rare. We also note that the pressure-dependent shape of the *Arridge et al.* [2006] magnetopause model implies that our approach, which constrains the shape of the shock to be constant, may not be appropriate for projecting shock standoff distances. We suggest that the projected standoff distances of crossings that occurred far from the subsolar region should be treated with a degree of caution.

4. Discussion

[36] In constructing this new empirical model a number of assumptions have been made; in this section we examine the validity of those assumptions. To justify the assumed upstream solar wind speed for the Cassini crossings and the assumed bow shock response to upstream solar wind dynamic pressure variations we calculated a conic section fit to the crossing set using an optimization routine. In the routine the assumed solar wind speed and power law constant c_2 were set as free parameters in order to test these two assumptions. In addition, to test the assumption that spacecraft trajectory effects do not bias the new empirical model a reduced set of crossings was considered and a conic section was constructed using the same approach used to construct the new empirical model. In each case the resulting conic section was compared to the new model to test the validity of the assumption(s) in question. After this discussion of the assumptions we compare the new empirical model to the existing models of Saturn's bow shock and comment on the similarities and differences.

4.1. Validating the Assumptions

[37] To test the assumptions of a solar wind speed of (500 ± 100) km s^{-1} upstream of all the Cassini crossings and a bow shock power law constant c_2 of 4.3 both were treated as free parameters. By combining the power law with the equation of a conic section, where the focus is at the center of the planet (equations (1) and (2)), we obtain equation (5) which gives the radial distance to a shock crossing for a specific solar wind dynamic pressure and polar coordinate angle, dependent on the values of the parameters ε, c_1, and c_2. The symbols represent the same quantities as for equations (1)–(4):

$$r = \frac{(1+\varepsilon)c_1 P_{SW}{}^{-1/c_2}}{1+\varepsilon\cos\theta}. \tag{5}$$

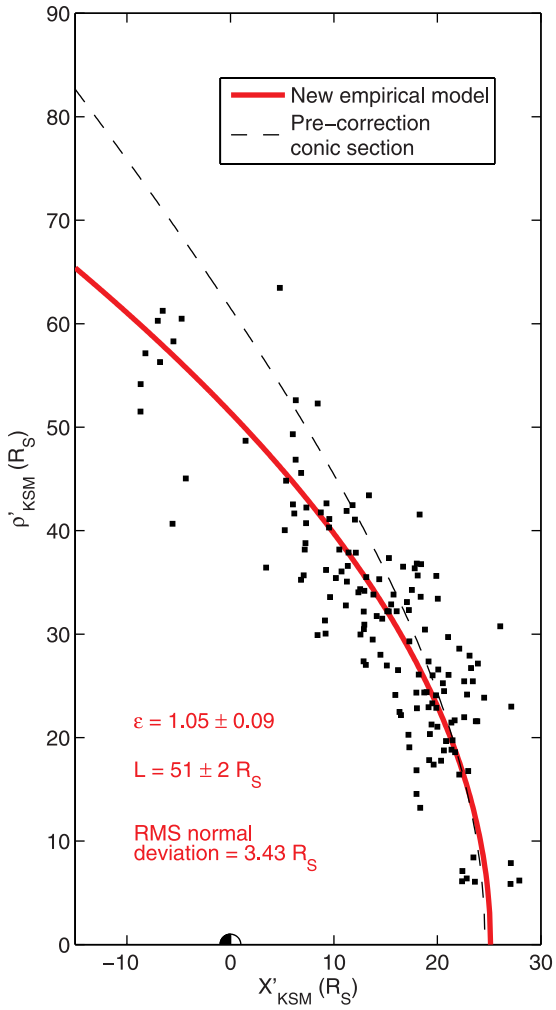

Figure 7. The positions of the bow shock crossings used in the construction of the model after the correction for solar wind dynamic pressure variation projected into the aberrated x-ρ plane. The new empirical model is shown, and its parameters are given. The best fit conic section before the pressure correction is also shown for comparison.

[38] The assumed solar wind flow speed, v_{sw}, was introduced as a fourth parameter that was used in the estimation of the value of P_{SW} for each Cassini crossing, thus for given values of the parameters the radial distance to each crossing at its observed polar coordinate angle is predicted and can then be compared to the observed value. To determine the values of the parameters that were a best fit to the observations an unconstrained nonlinear optimization routine based on the Nelder-Mead method [*Nelder and Mead*, 1965] was used. Initial values of the parameters were chosen and the routine iterated to determine the parameter values that minimized the RMS difference between the predicted and observed radial distances to the crossings; these optimized parameters are shown in Figure 8 as well as the associated pressure-corrected crossing positions and conic section. To calculate the uncertainties in the optimized parameters the Monte Carlo method employed by *Arridge et al.* [2006] was used. The fitting was repeated 200 times where at each iteration 80% of the total number of crossings were chosen randomly with replacement and used in the fitting routine. The standard deviation of the resulting distribution of each optimized parameter was taken as the error in that parameter. We considered a range of initial parameter values and found that the optimized parameters were very stable to changes in these initial conditions, and were within the uncertainties quoted in Figure 8.

[39] In Figure 8 the new empirical model is also shown for comparison with the result of the optimization routine; it is evident that the two conic sections are similar. Quantitatively, the values of the eccentricity and size parameter of the optimization technique conic section shown in Figure 8 are within errors of those of the new empirical model, shown in Figure 7. Although the optimized solar wind speed and power law constant c_2 are not within errors of the values that we have assumed they result in a conic section that is within errors of that of the new model, this indicates that the new empirical model is not sensitive to changes in these assumed parameters. Thus we suggest that

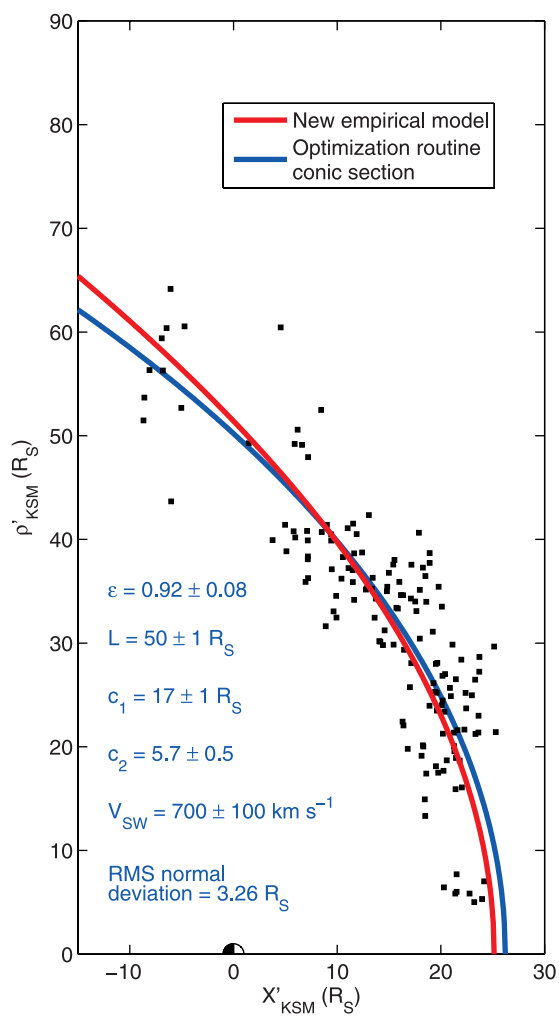

Figure 8. The conic section resulting from the optimization routine. The values of the optimized parameters are given, and the resulting pressure-corrected crossing positions and optimization conic section are shown in the aberrated x-ρ plane. The new empirical model conic section is also shown for comparison.

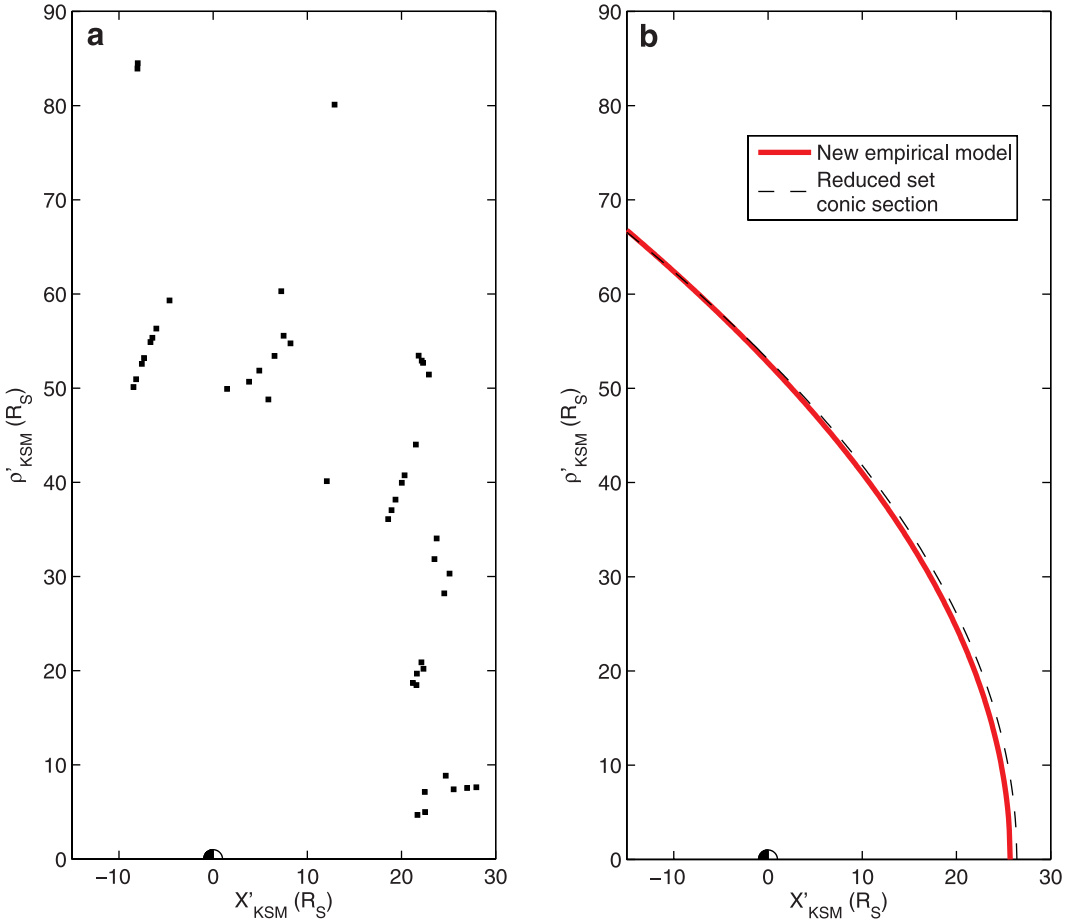

Figure 9. The results of the investigation into trajectory biasing of the model. (a) The positions of the reduced set of crossings projected into the aberrated x-ρ plane. (b) The new empirical model conic section and conic section resulting from the use of the reduced set projected into the aberrated x-ρ plane for comparison.

our assumptions of a particular solar wind velocity upstream of the Cassini crossings and bow shock response to solar wind dynamic pressure variations are valid, since changes in the assumed values do not significantly affect the resulting conic section.

[40] To construct the new empirical model, in the absence of upstream solar wind dynamic pressure measurements for the majority of the crossings, we have made a number of assumptions in order to use the conventional approach. However, we note that by introducing two additional free parameters (v_{sw} and c_2) the optimization routine approach avoids these assumptions and results in a conic section with a corresponding RMS normal deviation of 3.26 R_S; this is 5.0% less than the 3.43 R_S deviation associated with the new model obtained using the conventional approach. Since the optimized value of the assumed solar wind speed does not lie within the range of the measurements presented by *Crary et al.* [2005], and the resulting conic section is within errors of the new model, the conventional approach has been preferred in this study. Although in this instance the optimization approach has only been used to justify the assumptions, in future studies of planetary bow shocks such an approach may be preferable if upstream dynamic pressure measurements are unavailable.

[41] To address the assumption that spacecraft trajectory effects do not bias the model a reduced set of crossings was used to determine a conic section using exactly the same approach used in the model's construction. Since a relatively large number of shock crossings occurred in the sixth and subsequent Cassini orbits our reduced set was composed of the crossings that were made during the first five Cassini orbits, combined with the Pioneer and Voyager crossings. The total number of crossings in this reduced set is 47; when pressure correcting the crossing positions the average solar wind dynamic pressure of 0.039 nPa for the reduced set was used which is not the same as the average pressure for the entire set used in the construction of the new model. Figure 9a shows the distribution of the crossings in the reduced set before the correction for dynamic pressure variation, whereas Figure 9b compares the conic section obtained using the reduced set to the new model which used the full set of crossings. In Figure 9b the reduced set conic section has been scaled to the dynamic pressure of 0.048 nPa corresponding to the new model using equation (4) in order to make a valid comparison. There is a negligible difference between the two conic sections and thus we suggest that the assumption that spacecraft trajectory effects do not bias the model is justified.

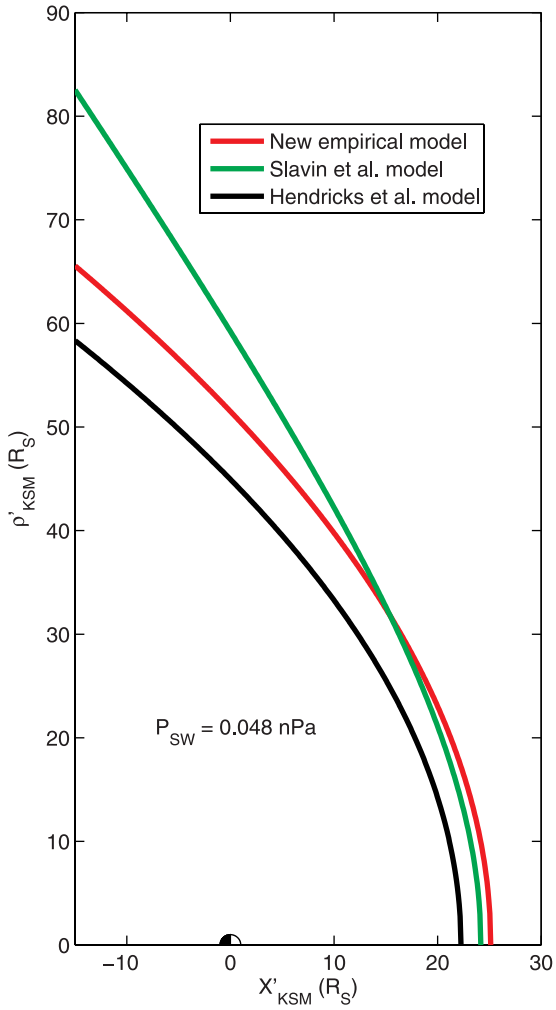

Figure 10. A comparison between the locations of the bow shock predicted by the new empirical model and the existing models [*Slavin et al.*, 1985; *Hendricks et al.*, 2005] projected into the aberrated x-ρ plane for a specified solar wind dynamic pressure.

[42] When calculating the best fit conic section to the distribution of crossing positions before and after the dynamic pressure correction we made an additional assumption. Unlike many previous studies [e.g., *Slavin and Holzer*, 1981] the focus of the conic section was fixed at the center of the planet and not allowed to have a variable position on the aberrated x axis. To examine the validity of this assumption we recalculated the best fit conic section to the precorrection and postcorrection distribution allowing the focus position on the aberrated x axis to be a free parameter. For the distribution before the pressure correction (shown in Figure 5) we obtained an eccentricity of (1.6 ± 0.3) a size parameter of (59 ± 5) R_S and an aberrated x axis focus position of (2.0 ± 0.4) R_S with an RMS normal deviation of 5.38 R_S. For the distribution after the pressure correction (shown in Figure 7) we obtained an eccentricity of (1.06 ± 0.09) a size parameter of (51 ± 2) R_S and an aberrated x axis focus position of (0.4 ± 0.1) R_S with an RMS normal deviation of 3.43 R_S. In both cases the eccentricity and size parameter are well within errors of the values obtained with a fixed focus position. The difference between the RMS normal deviations, as a percentage of the RMS normal deviation associated with the conic section with a fixed focus position, is 0.01% for the precorrection distribution and 0.001% for the postcorrection distribution. On the basis of these calculations we conclude that the assumption that the focus position of the conic sections is at the center of the planet is valid.

[43] As the crossings used in this study occurred at low latitudes predominantly in the dawn sector our model describes this part of the bow shock surface, as a result we are not able to address the remaining assumption that the bow shock surface is axially symmetric about the solar wind flow direction. Future analysis of higher-latitude crossings in more recent Cassini orbits may reveal a departure from axis symmetry.

4.2. Comparison With Existing Models

[44] The bow shock locations predicted by the existing models and the new empirical model described in this paper are shown for a specified value of the solar wind dynamic pressure in Figure 10; there are distinct similarities and differences between the new model and the *Slavin et al.* [1985] and *Hendricks et al.* [2005] models. It is clear in Figure 10 that the *Slavin et al.* [1985] model is considerably more flared than the new model, since their model eccentricity of 1.71 is far greater than the value of 1.05 for the new model. The greatest difference between the bow shock location predicted by the *Slavin et al.* [1985] model and the new model is on the dawn flank rather than in the subsolar region, which we suggest is due to the limited number and local time coverage of the Pioneer and Voyager crossings used in the construction of their model. The new model is able to build a considerably clearer picture of the global shock location and shape as it is based on a far greater number of crossings over a greater range of local times.

[45] The (1.05 ± 0.09) value of the eccentricity of the new empirical model is within errors of the 1.02 value for the *Hendricks et al.* [2005] theoretical model, however the predictions of the position of the shock at a given solar wind dynamic pressure are markedly different, as shown in Figure 10. This is due to the differences in the model power laws; the *Hendricks et al.* [2005] model power law has a compressibility that is more Earth-like than the new empirical model which is more Jupiter-like in that respect. *Hansen et al.* [2005] have carried out a recent global MHD simulation of Saturn's magnetosphere during Cassini's approach to the planet in mid-2004, a preliminary visual comparison with their results for the bow shock location suggests an agreement with the extent of flaring of the new empirical model, although they calculate a bow shock power law constant c_2 of 5.9 which is markedly different from the value of 4.3 assumed in the new model. A more detailed and extensive comparison between such simulations and the new model would be of benefit to our understanding of the global configuration and dynamics of the shock.

[46] The Cassini observations have implied that the magnetosphere is more compressible than previously thought [*Arridge et al.*, 2006], which is possibly due to the importance of inertial stresses in the magnetodisc current sheet [*Arridge et al.*, 2007; *Bunce et al.*, 2007].

We propose that this is taken into account by the new empirical model and thus it is the most accurate representation of the shape and location of the bow shock surface. Regarding the applicability of the new model we note that it only applies to a specific range of solar wind dynamic pressures. The range of the dynamic pressure measurements and estimates used in the construction of the new model was from 0.0033 to 0.19 nPa and thus the new model is appropriate for describing the global shape and location of the bow shock at dynamic pressures within this range, however for pressures beyond the limits of this range the model is not applicable. In addition, since the new model is based on extended observations of the bow shock location made during a period of approximately 15 months it describes the average shape and location of the boundary during this period. In the case of rapid, relatively large variations of the solar wind dynamic pressure, corresponding to magnetospheric expansion or contraction, departures from the bow shock position predicted by the new model are anticipated.

5. Conclusions

[47] A new empirical model of Saturn's bow shock that utilizes the Cassini observations has been presented. In the absence of an upstream monitor the solar wind dynamic pressure for all Cassini bow shock crossing was estimated by assuming a constant solar wind speed and using upstream electron number density measurements made by RPWS; furthermore, it was assumed that the response of the magnetopause and bow shock boundaries to changes in the dynamic pressure is the same. The positions of the crossings were modified to correct for the effects of planetary orbital motion and solar wind dynamic pressure variation and the resulting crossing positions were then used to construct the new empirical model, described by a conic section and an associated power law relation between bow shock standoff distance and solar wind dynamic pressure. To provide justification for the new model a number of the assumptions made in its construction were then validated. By employing an optimization routine with four free parameters it was shown that the model is not sensitive to changes in the assumed solar wind speed or bow shock response to solar wind dynamic pressure variations, this suggests that the assumed values are valid for the purposes of this study. By using a reduced set of crossings and determining a conic section using the same approach used to construct the new model it was also demonstrated that the new model is not trajectory biased, as there was a negligible difference between this conic section and that of the new model. Finally, the new empirical model has been compared to the existing models and the similarities and differences were discussed. Owing to the large number of crossings used, relative to previous studies, the new empirical model presented in this paper provides a clearer picture of the global shock surface and thus we suggest that it is the most accurate representation of the shape and location of Saturn's bow shock to date.

[48] A possibility for future work related to this study involves the calculation of a probability distribution for the bow shock location. *Joy et al.* [2002] calculated such distributions for the Jovian magnetopause and bow shock and found that the magnetopause distribution was bimodal, whereas the bow shock distribution appeared to be bimodal but a single distribution function could not be ruled out. They considered whether the bimodal magnetopause distribution was caused by a bimodal distribution of solar wind parameters at Jupiter for the period considered due to corotating interaction regions; however they found that the bimodal distribution could not be fully explained by the solar wind distribution function. They concluded that internal processes must be important contributors to the size and shape of the Jovian magnetosphere. *Achilleos et al.* [2008] have conducted a similar study for the Kronian magnetopause and have also found a bimodal distribution that could also either be attributed to a corotating interaction region dominated heliospheric structure at Saturn orbit for the period considered [*Jackman et al.*, 2004] or internal processes.

[49] The new empirical bow shock model has direct implications for the extent of north-south flattening of Saturn's magnetosphere. Owing to the presence of a magnetodisc it is anticipated that Saturn's magnetosphere is flattened in the polar direction, however until recently the lack of high-latitude magnetopause and bow shock crossings has prevented the investigation of this effect by the approach used by *Huddleston et al.* [1998] to examine the same phenomenon at Jupiter. By considering crossings of the Jovian boundaries in different ranges of magnetic latitude they were able to show that the average magnetopause was flattened in the north-south direction about the magnetic equator, although they found that no such flattening of the average bow shock surface was evident. The degree of polar flattening of a planetary magnetosphere can also be inferred by comparing empirical models of the low-latitude boundaries to the results of gas dynamic and MHD simulations [*Slavin et al.*, 1983; *Stahara et al.*, 1989; *Hansen et al.*, 2000, 2005] (see the review by *Spreiter and Stahara* [1995]). *Slavin et al.* [1985] compared their models of Saturn's low-latitude magnetopause and bow shock to the results of gas dynamic simulations and found that the subsolar magnetosheath was 20% thinner than that predicted by gas dynamic theory, where no polar flattening was present. This suggests a polar flattened magnetosphere and they concluded that the effect at Saturn was intermediate between that at Earth and Jupiter. During recent Cassini orbits crossings of both the magnetopause and bow shock have been made at higher latitudes than ever before; by combining these high-latitude boundary observations with a comparison between the Cassini era empirical models and simulations the extent of this polar flattening can be investigated. Such a study would be important for our understanding of the nature of the solar wind flow around Saturn's magnetosphere.

[50] **Acknowledgments.** A. M. acknowledges useful discussions with E. M. Henley, L. Billingham, and T. S. Horbury, as well as the support of the Royal Astronomical Society. This research has made use of NASA's Planetary Data System. We acknowledge the support of the MAG data processing/distribution staff and L. K. Gilbert and G. R. Lewis for ELS data processing. The research at the University of Iowa was supported by the National Aeronautics and Space Administration through contract 1279973 with the Jet Propulsion Laboratory. This work was supported by UK STFC through the award of a studentship (A. M.) and rolling grants to MSSL/UCL and Imperial College London.

[51] Amitava Bhattacharjee thanks Steven P. Joy for his assistance in evaluating this paper.

References

Achilleos, N., et al. (2006), Orientation, location and velocity of Saturn's bow shock: Initial results from the Cassini spacecraft, *J. Geophys. Res.*, *111*, A03201, doi:10.1029/2005JA011297.

Achilleos, N., C. S. Arridge, C. L. Bertucci, C. M. Jackman, M. K. Dougherty, M. K. Khurana, and C. T. Russell (2008), Large-scale dynamics of Saturn's magnetopause: Observations by Cassini, *J. Geophys. Res.*, doi:10.1029/2008JA013265, in press.

Acuña, M. H., and N. F. Ness (1980), The magnetic field of Saturn: Pioneer 11 observations, *Science*, *207*, 444–446, doi:10.1126/science.207.4429.444.

Arridge, C. S. (2007), On the configuration and dynamics of Saturn's magnetosphere, Ph.D. thesis, Univ. of London, London, U.K.

Arridge, C. S., N. Achilleos, M. K. Dougherty, K. K. Khurana, and C. T. Russell (2006), Modeling the size and shape of Saturn's magnetopause with variable dynamic pressure, *J. Geophys. Res.*, *111*, A11227, doi:10.1029/2005JA011574.

Arridge, C. S., C. T. Russell, K. K. Khurana, N. Achilleos, N. André, A. M. Rymer, M. K. Dougherty, and A. J. Coates (2007), Mass of Saturn's magnetodisc: Cassini observations, *Geophys. Res. Lett.*, *34*, L09108, doi:10.1029/2006GL028921.

Arridge, C. S., C. T. Russell, K. K. Khurana, N. Achilleos, S. W. H. Cowley, M. K. Dougherty, D. J. Southwood, and E. J. Bunce (2008), Saturn's magnetodisc current sheet, *J. Geophys. Res.*, *113*, A04214, doi:10.1029/2007JA012540.

Bale, S. D., et al. (2005), Quasi-perpendicular shock structure and processes, *Space Sci. Rev.*, *118*, 161, doi:10.1007/s11214-005-3827-0.

Behannon, K. W., R. P. Lepping, and N. F. Ness (1983), Structure and dynamics of Saturn's outer magnetosphere and boundary regions, *J. Geophys. Res.*, *88*, 8791.

Bennett, L., M. G. Kivelson, and K. K. Khurana (1997), A model of the Earth's distant bow shock, *J. Geophys. Res.*, *102*, 26,927.

Binsack, J. H., and V. M. Vasyliunas (1968), Simultaneous IMP 2 and OGO 1 observations of bow shock compression, *J. Geophys. Res.*, *73*, 429.

Bridge, H. S., et al. (1981), Plasma observations near Saturn: Initial results from Voyager 1, *Science*, *212*, 217, doi:10.1126/science.212.4491.217.

Bridge, H. S., et al. (1982), Plasma observations near Saturn: Initial results from Voyager 2, *Science*, *215*, 563, doi:10.1126/science.215.4532.563.

Bunce, E. J., S. W. H. Cowley, I. I. Alexeev, C. S. Arridge, M. K. Dougherty, J. D. Nichols, and C. T. Russell (2007), Cassini observations of the variation of Saturn's ring current parameters with system size, *J. Geophys. Res.*, *112*, A10202, doi:10.1029/2007JA012275.

Burgess, D. (1995), Collisionless shocks, in *Introduction to Space Physics*, edited by M. G. Kivelson and C. T. Russell, pp. 129–163, Cambridge Univ. Press, New York.

Burgess, D., et al. (2005), Quasi-parallel shock structure and processes, *Space Sci. Rev.*, *118*, 205, doi:10.1007/s11214-005-3832-3.

Cairns, I. H., W. S. Kurth, D. A. Gurnett, C. W. Smith, and S. Moses (1991), Remote sensing of Neptune's bow shock: Evidence for large-scale shock motions, *J. Geophys. Res.*, *96*, 19,153.

Connerney, J. E. P., N. F. Ness, and M. H. Acuña (1982), Zonal harmonic model of Saturn's magnetic field from Voyager 1 and 2 observations, *Nature*, *298*, 44, doi:10.1038/298044a0.

Crary, F. J., et al. (2005), Solar wind dynamic pressure and electric field as the main factors controlling Saturn's aurorae, *Nature*, *433*, 720, doi:10.1038/nature03333.

Dougherty, M. K., et al. (2004), The Cassini magnetic field investigation, *Space Sci. Rev.*, *114*, 331, doi:10.1007/s11214-004-1432-2.

Eastwood, J. P. (2003), The terrestrial foreshock as observed by the multi-spacecraft Cluster mission, Ph.D. thesis, Univ. of London, London, U.K.

Fairfield, D. H. (1971), Average and unusual locations for the Earth's magnetopause and bow shock, *J. Geophys. Res.*, *76*, 6700.

Farris, M. H., and C. T. Russell (1994), Determining the standoff distance of the bow shock: Mach number dependence and use of models, *J. Geophys. Res.*, *99*, 17,681.

Farris, M. H., S. M. Petrinec, and C. T. Russell (1991), The thickness of the magnetosheath: Constraints on the polytropic index, *Geophys. Res. Lett.*, *18*, 1821.

Formisano, V. (1979), Orientation and shape of the Earth's bow shock in three dimensions, *Planet. Space Sci.*, *27*, 1151, doi:10.1016/0032-0633(79)90135-1.

Gosling, J. T., and A. E. Robson (1985), Ion reflection, gyration, and dissipation at supercritical shocks, in *Collisionless Shocks in the Heliosphere: Reviews of Current Research*, *Geophys. Monogr. Ser.*, vol. 35, edited by B. T. Tsurutani and R. G. Stone, 141 pp., AGU, Washington, D. C.

Gurnett, D. A., et al. (2004), The Cassini Radio and Plasma Wave Investigation, *Space Sci. Rev.*, *114*, 395, doi:10.1007/s11214-004-1434-0.

Hansen, K. C., T. I. Gombosi, D. L. DeZeeuw, C. P. T. Groth, and K. G. Powell (2000), A 3D global MHD simulation of Saturn's magnetosphere, *Adv. Space Res.*, *26*, 1681, doi:10.1016/S0273-1177(00)00078-8.

Hansen, K. C., A. J. Ridley, G. B. Hospodarsky, N. Achilleos, M. K. Dougherty, T. I. Gombosi, and G. Tóth (2005), Global MHD simulations of Saturn's magnetosphere at the time of Cassini approach, *Geophys. Res. Lett.*, *32*, L20S06, doi:10.1029/2005GL022835.

Hendricks, S., F. M. Neubauer, M. K. Dougherty, N. Achilleos, and C. T. Russell (2005), Variability in Saturn's bow shock and magnetopause from Pioneer and Voyager: Probabilistic predictions and initial observations by Cassini, *Geophys. Res. Lett.*, *32*, L20S08, doi:10.1029/2005GL022569.

Huddleston, D. E., C. T. Russell, M. G. Kivelson, K. K. Khurana, and L. Bennett (1998), Location and shape of the Jovian magnetopause and bow shock, *J. Geophys. Res.*, *103*, 20,075.

Ishisaka, K. T., et al. (2001), Relationship between the Geotail spacecraft potential and the magnetospheric electron number density including the distant tail regions, *J. Geophys. Res.*, *106*, 6309.

Jackman, C. M., N. Achilleos, E. J. Bunce, S. W. H. Cowley, M. K. Dougherty, G. H. Jones, S. E. Milan, and E. J. Smith (2004), Interplanetary magnetic field at ~9 AU during the declining phase of the solar cycle and its implications for Saturn's magnetospheric dynamics, *J. Geophys. Res.*, *109*, A11203, doi:10.1029/2004JA010614.

Jackman, C. M., R. J. Forsyth, and M. K. Dougherty (2008), The overall configuration of the interplanetary magnetic field upstream of Saturn, as revealed by Cassini observations, *J. Geophys. Res.*, *113*, A08114, doi:10.1029/2008JA013083.

Joy, S. P., M. G. Kivelson, R. J. Walker, K. K. Khurana, C. T. Russell, and T. Ogino (2002), Probabilistic models of the Jovian magnetopause and bow shock locations, *J. Geophys. Res.*, *107*(A10), 1309, doi:10.1029/2001JA009146.

Khurana, K. K., and M. G. Kivelson (1994), A variable cross-section model of the bow shock of Venus, *J. Geophys. Res.*, *99*, 8505.

Masters, A., C. S. Arridge, M. K. Dougherty, C. Bertucci, L. Billingham, S. J. Schwartz, C. M. Jackman, Z. Bebesi, A. J. Coates, and M. F. Thomsen (2008), Cassini encounters with hot flow anomaly-like phenomena at Saturn's bow shock, *Geophys. Res. Lett.*, *35*, L02202, doi:10.1029/2007GL032371.

Matson, D. L., L. J. Spilker, and J.-P. Lebreton (2002), The Cassini/Huygens mission to the Saturnian system, *Space Sci. Rev.*, *104*, 1, doi:10.1023/A:1023609211620.

Maurice, S., I. Engle, M. Blanc, and M. Skubis (1996), Geometry of Saturn's magnetopause model, *J. Geophys. Res.*, *101*, 27,053.

Merka, J., A. Szabo, J. A. Slavin, and M. Peredo (2005), Three-dimensional position and shape of the bow shock and their variation with upstream Mach numbers and interplanetary magnetic field orientation, *J. Geophys. Res.*, *110*, A04202, doi:10.1029/2004JA010944.

Nelder, J. A., and R. Mead (1965), A simplex method for function minimization, *Comput. J.*, *7*, 308.

Ness, N. F., M. H. Acuña, R. P. Lepping, J. E. P. Connerney, K. W. Behannon, L. F. Burlaga, and F. M. Neubauer (1981), Magnetic field studies by Voyager 1: Preliminary results at Saturn, *Science*, *212*, 211, doi:10.1126/science.212.4491.211.

Ness, N. F., M. H. Acuña, K. W. Behannon, L. F. Burlaga, J. E. P. Connerney, R. P. Lepping, and F. M. Neubauer (1982), Magnetic field studies by Voyager 2: Preliminary results at Saturn, *Science*, *215*, 558, doi:10.1126/science.215.4532.558.

Petrinec, S. M., and C. T. Russell (1993), External and internal influences on the size of the dayside terrestrial magnetosphere, *Geophys. Res. Lett.*, *20*, 339.

Petrinec, S. M., and C. T. Russell (1997), Hydrodynamic and MHD equations across the bow shock and along the surfaces of planetary obstacles, *Space Sci. Rev.*, *79*, 757, doi:10.1023/A:1004938724300.

Russell, C. T. (1985), Planetary bow shocks, in *Collisionless Shocks in the Heliosphere: Reviews of Current Research*, *Geophys. Monogr. Ser.*, vol. 35, edited by B. T. Tsurutani and R. G. Stone, 109 pp., AGU, Washington, D. C.

Slavin, J. A., and R. E. Holzer (1981), Solar wind flow about the terrestrial planets: 1. Modeling bow shock position and shape, *J. Geophys. Res.*, *86*, 11,401.

Slavin, J. A., R. C. Elphic, C. T. Russell, J. H. Wolfe, and D. S. Intriligator (1979), Position and shape of the Venus bow shock: Pioneer Venus Orbiter observations, *Geophys. Res. Lett.*, *6*, 901.

Slavin, J. A., R. C. Elphic, C. T. Russell, F. L. Scarf, J. H. Wolfe, J. D. Mihalov, D. S. Intriligator, L. H. Brace, H. A. Taylor, and R. E. Daniell (1980), The solar wind interaction with Venus: Pioneer Venus observations of bow shock location and structure, *J. Geophys. Res.*, *85*, 7625.

Slavin, J. A., R. E. Holzer, J. R. Spreiter, S. S. Stahara, and D. S. Chaussee (1983), Solar wind flow about the terrestrial planets: 2. Comparison with

gas dynamic theory and implications for solar-planetary interactions, *J. Geophys. Res.*, *88*, 19.

Slavin, J. A., R. E. Holzer, J. R. Spreiter, and S. S. Stahara (1984), Planetary Mach cones: Theory and observation, *J. Geophys. Res.*, *89*, 2708.

Slavin, J. A., E. J. Smith, J. R. Spreiter, and S. S. Stahara (1985), Solar wind flow about the outer planets: Gas dynamic modeling of the Jupiter and Saturn bow shocks, *J. Geophys. Res.*, *90*, 6275.

Smith, E. J., L. Davis Jr., D. E. Jones, P. J. Coleman Jr., D. S. Colburn, P. Dyal, and C. P. Sonett (1980), Saturn's magnetosphere and its interaction with the solar wind, *J. Geophys. Res.*, *85*, 5655.

Spreiter, J. R., and S. S. Stahara (1995), The location of planetary bow shocks: A critical overview of theory and observations, *Adv. Space Res.*, *15*, 433, doi:10.1016/0273-1177(94)00128-N.

Stahara, S. S., R. R. Rachiele, J. R. Spreiter, and J. A. Slavin (1989), A three dimensional gasdynamic model for solar wind flow past nonaxisymmetric magnetospheres: Application to Jupiter and Saturn, *J. Geophys. Res.*, *94*, 13,353.

Stone, E. C., and E. D. Miner (1981), Voyager 1 encounter with the Saturnian system, *Science*, *212*, 159, doi:10.1126/science.212.4491.159.

Stone, E. C., and E. D. Miner (1982), Voyager 2 encounter with the Saturnian system, *Science*, *215*, 499, doi:10.1126/science.215.4532.499.

Walker, R. J., and C. T. Russell (1995), Solar-wind interactions with magnetized planets, in *Introduction to Space Physics*, edited by M. G. Kivelson and C. T. Russell, pp. 164–181, Cambridge Univ. Press, New York.

Young, D. T., et al. (2004), Cassini Plasma Spectrometer Investigation, *Space Sci. Rev.*, *114*, 1, doi:10.1007/s11214-004-1406-4.

Young, D. T., et al. (2005), Composition and dynamics of plasma in Saturn's magnetosphere, *Science*, *307*, 1262, doi:10.1126/science.1106151.

N. Achilleos, Atmospheric Physics Laboratory, Department of Physics and Astronomy, University College London, Gower Street, London WC1E 6BT, UK.

C. S. Arridge and A. J. Coates, Mullard Space Science Laboratory, Department of Space and Climate Physics, University College London, Holmbury St. Mary, Dorking RH5 6NT, UK.

M. K. Dougherty and A. Masters, Space and Atmospheric Physics Group, The Blackett Laboratory, Imperial College London, Prince Consort Road, London SW7 2BW, UK. (adam.masters02@imperial.ac.uk)

G. B. Hospodarsky, Department of Physics and Astronomy, University of Iowa, Iowa City, IA 52242, USA.

J. A. Slavin, Heliophysics Science Division, NASA GSFC, Greenbelt, MD 20771, USA.